Thermomechancial Characterization in a Radiant Energy Imager Using Null Switching

Javaneh Boroumand, Imen Rezadad, Ammar Alhasan, Evan Smith, Robert E. Peale
Department of Physics, University of Central Florida, Orlando, FL, USA 32816

Abstract

Thermomechanical noise for a MEMs-based infrared detector using null switching (US patent 7977635) depends on vibrational amplitude, since IR radiation is transduced to a change in the duty cycle of a repetitively closing switch. Equipartition theorem determines the maximum rms vibrational amplitude for the fabricated cantilever switch at its natural frequency. This determines the timing uncertainty, NEP, and NETD. We estimate NETD to fall in the range 0.13 – 1.5 K for a device with ~20 μm pitch.

Key words: MEMs, thermal, Infrared, noise

1. INTRODUCTION

This paper discusses thermo-mechanical noise for an infrared detector device invented by Oliver Edwards[1]. This detector is unusual in that absorbed IR radiation is transduced into a measurement of a time. High sensitivity to small differences in scene temperature requires high measurement bandwidth. Thermomechanical noise is determined by this bandwidth rather than by the frame rate, as in usual imaging detectors. Thus, the vibrational amplitude at the cantilever's natural oscillation frequency is important.

A simplified schematic of the MEMS cantilever device is presented in Fig. 1. The tip of the cantilever consists of a tip contact that is normally touching a surface tip pad ("null position"), allowing electrical sensing of contact. An upward electrostatic force F_{ES} appears when the device is biased as shown[2,3]. This is opposed by an elastic restoring force F_E and a sticking force F_C such as Casimir force[3,4]. The latter force will be ignored here. For simplicity we will consider the elastic force to apply mainly to the arms and we ignore any deformation of the metal-coated regions.
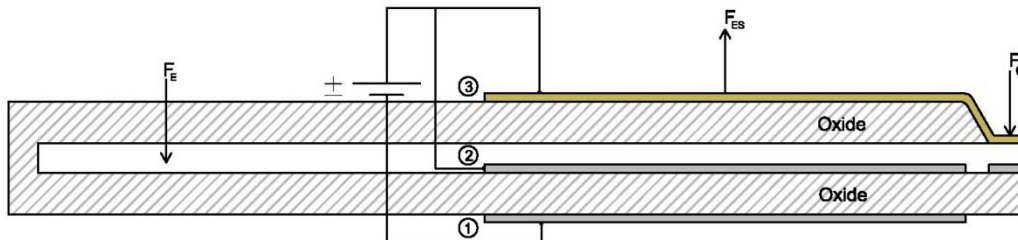

Fig. 1. Schematic of MEMS cantilever device.

The structural material is silicon dioxide. The entire top surface of the cantilever, including the arms is coated with a thin layer of metal. Fig. 2 presents a scanning electron microscope image of a 3x3 array of such devices fabricated by our group at UCF. The sections of the arms that is connected to the absorber plate has an additional thickness of metal to form a thermal bimorph that bends concave downwards when the device is heated by absorbed IR radiation. The length of the bimorph arms is 18 microns. An elbow connects the bimorph arms to isolation arms, which are anchored to the substrate and electrically connected to a metal surface plate. The width of each segment of the arms is 2 microns. The thickness of the structural oxide in the arms is 0.4 microns.
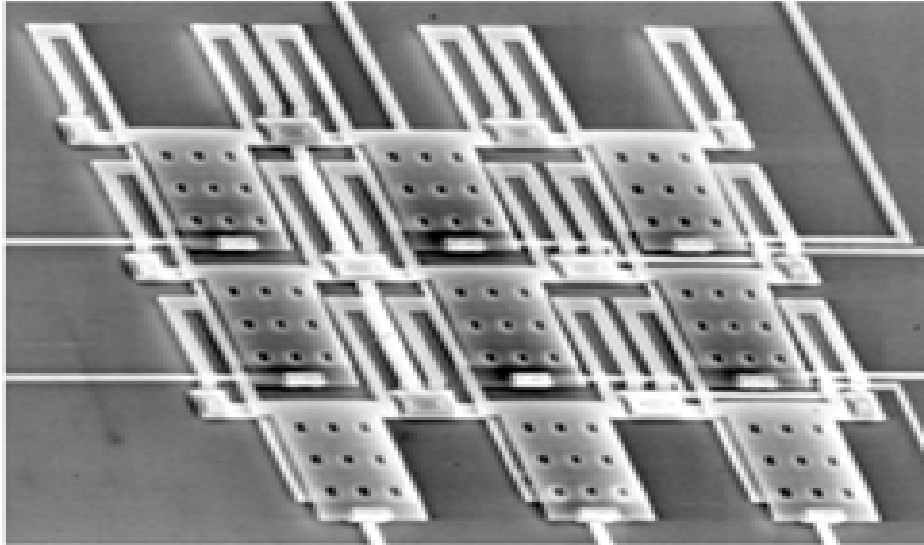
Fig. 2. SEM image of MEMS cantilever IR sensor array. Paddles are 18 μm x 20 μm.

Fig. 3 presents a schematic of the applied and measured voltage waveforms. In equilibrium the free end of the cantilever is in physical and electrical contact with the tip pad. When the cantilever is biased with a voltage V_B, an upwards repulsive electrostatic force lifts the cantilever from the surface and breaks the tip contact. As V_B is ramped down during a time τ, the voltage at the tip contact V_T is monitored. If IR radiation is absorbed, thermal deformation of the bimorph arms causes the tip to return to the tip contact sooner than τ by a time $\Delta\tau$, as determined by the voltage V_T that appears on contact. The time $\Delta\tau$ gives a temporal measurement of the absorbed IR flux. Thermo-mechanical vibration of the cantilever results in uncertainty in the time of contact, and hence noise in the determination of IR flux[5].
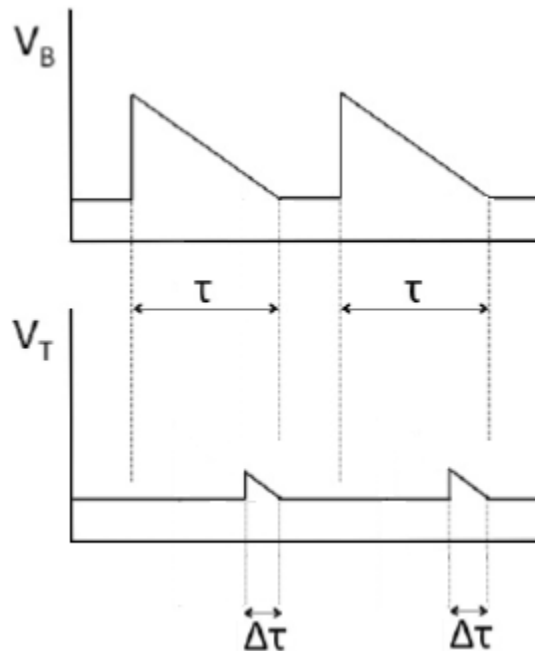

Fig. 3. Timing diagram showing applied bias V_B and measured tip voltage V_T waveforms.

2. FABRICATION

The standard MEMS processing approach is presented schematically in Fig. 4. It starts with a blanket coat of Cr onto a silicon wafer to form the buried plate, which is isolated next by PECVD silicon dioxide from subsequent structures. A metal lift-off pattern forms the surface plate. The wafer is next spin-coated with a polyimide sacrificial layer (ProLift, Brewer Science). Co-development through a resist mask produces anchor holes through the sacrificial layer to the surface plate. Partial development forms divots in the ProLift, which are then filled with Cr to form the metal tips. A low-stress PECVD oxide blanket deposition is followed by patterned metal lift-off. RIE defines the cantilever using the patterned metal as etch mask. Electrical continuity between cantilever and surface plates, and between the cantilever and its underside tip metal, is achieved by a patterned metal deposition on the anchors and over the edge of the cantilever. RIE in O_2 plasma releases the pixels according to a UV-assisted process[6].
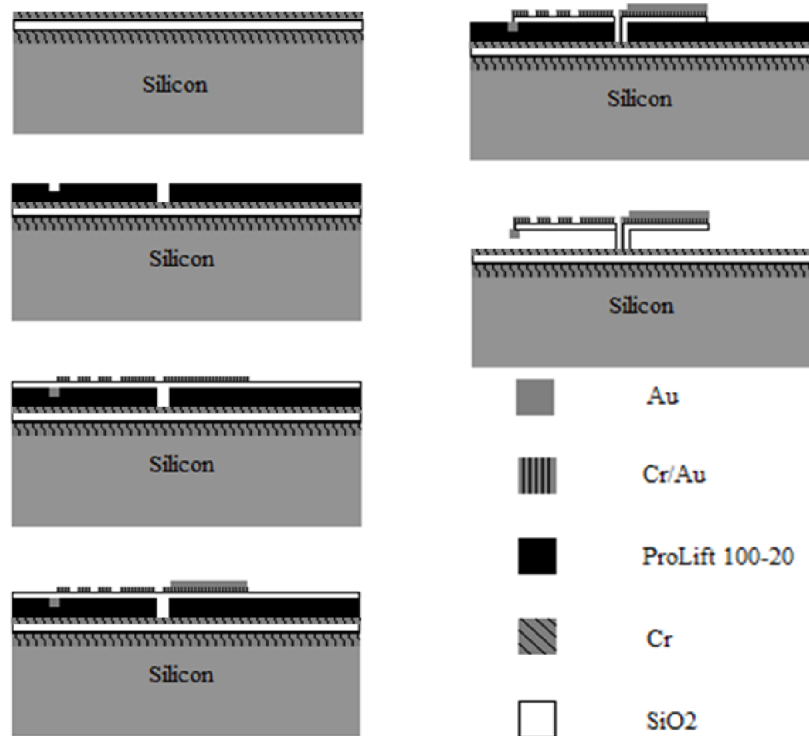
Fig. 4. Schematic of fabrication steps for MEMS cantilever detector.

3. FINITE ELEMENT METHOD CALCULATIONS

Key to the estimation of thermo-mechanical noise is an estimate of the spring constant of the cantilever, considered as a 1D simple harmonic oscillator. Figure 5 presents solved stress field and displacement of the cantilever. This particular calculation was done assuming Aluminum as the material, with Poisson ratio 0.35, Young's modulus 70 GPa, and density 2700 kg/m³. The cantilever is fixed to the substrate at its anchors. It is subjected to a stress of 154 N/m² as a result of uniformly distributed force on its 20 x 18 μm² area plates. Color indicates vertical displacement. Blue is the maximum displacement in the negative z direction, while white is the maximum displacement in positive z direction. The anchors are fixed at $z = 0$, which is color-coded light purple. For these calculations, the equilibrium position of the cantilever tip is at $z = 0$, in contrast to that actual device, where the cantilever in equilibrium is bent down with the tip touching the surface 2 μm below the anchor point for the isolation arms. This should make little difference in the value of the spring constant determined.

Fig. 5 shows that the elbows on the arms bend upward by ~10% of the amount that the tip bends down. From the top view color gradient, one sees that the bimorph arms (inner pair) have more curvature than the isolation arms (outer pair).

Thus, the elastic restoring force is primarily due to the inner pair of arms, a fact that will be considered in the analytic calculations below.

A plot of force as a function of displacement is linear. We find for an Aluminum cantilever that the spring constant K has the value 0.73 N/m. (Aluminum is considered for comparison to some macroscopic machined models that we experimented with to test the FEM results, see below.) For SiO_2, as in the actual cantilever, we used Poisson ratio 0.17, Young's modulus 70 GPa, and density 2200 kg/m³ to find K = 0.68 N/m.
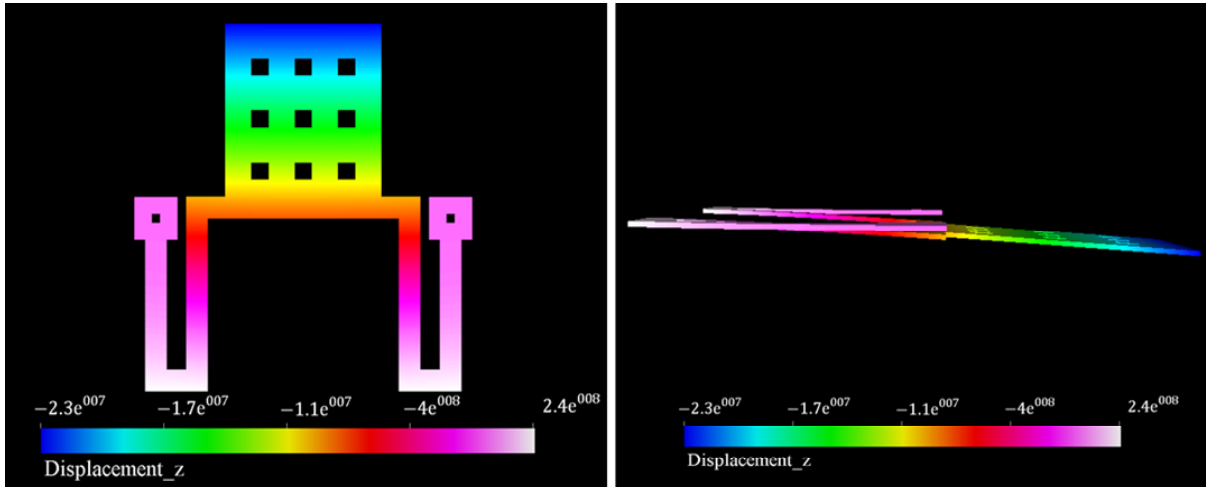

Fig. 5. (Left) Top view of deflection distribution due to the stress caused by uniformly applied pressure of 154 N/m² applied to the rigid 20 x 18 μm² cantilever plate. (Right) Side view of the cantilever displacement scaled up by a factor of 10.

4. THERMO-MECHANICAL NOISE

Suppose the cantilever is an undamped one-dimensional oscillator with natural frequency ω_0. The equipartition theorem indicates that the mean square amplitude of the vibrations should not be less than

$$(1/2)\ K <z^2> = (1/2)\ k_B\ T \qquad (1)$$

If we take the spring constant to have the value $K = 0.68$ N/m, we find the rms vibrational amplitude to be 79 pm at room temperature. This value is 4000x larger than the value given in [5] from a published thermomechanical noise formula assuming 30 Hz bandwidth. The reason for the difference is that 30 Hz is far from the ~240 kHz natural frequency of the cantilever (mass ~0.3 ng). The amplitude of oscillations at 30 Hz is small because this frequency is far out on the wing of the vibrational resonance line shape.

The detector mode of operation requires high electronic bandwidth to differentiate small timing differences that indicate small differences in scene temperature. Since timing measurements may be done with reference to quartz stable clocks operating easily at 20 MHz or more, the natural frequency of the cantilever will be within the measurement bandwidth. Thus, timing uncertainty (i.e. noise) is determined by the natural frequency where vibrational oscillations are maximum.

To illustrate, Fig. 6 presents the final 6.7 μs of the tip-height sawtooth with and without superimposed thermal noise at the natural frequency. The tip touches early by $\delta\tau = 0.7$ μs. We may demonstrate mathematically that the timing uncertainty depends primarily on noise amplitude as follows. For frame rate f and noise frequency ω, the tip height is

$$z(t) = z_0\ (1 - 2\ f\ t) + A\ \mathrm{Cos}[\omega t + \phi] \qquad . \qquad (2)$$

The time of contact is determined by setting the left side to zero and solving for t. When the noise amplitude $A = 0$, touch down occurs at time $\tau = 1/2f$ (50% duty is assumed). The maximum timing error occurs when Cos = ±1, for which the maximum timing uncertainty $\delta\tau = \pm A/(2\ f\ z_0)$. This timing uncertainty depends on amplitude A, but it does not

depend on ω. Thus, thermomechanical noise is mainly defined by noise at the natural frequency of the cantilever, where amplitude is largest. For $A = 79$ pm, $f = 30$ Hz and $z_0 = 2$ μm, we find $\delta\tau = 660$ ns.
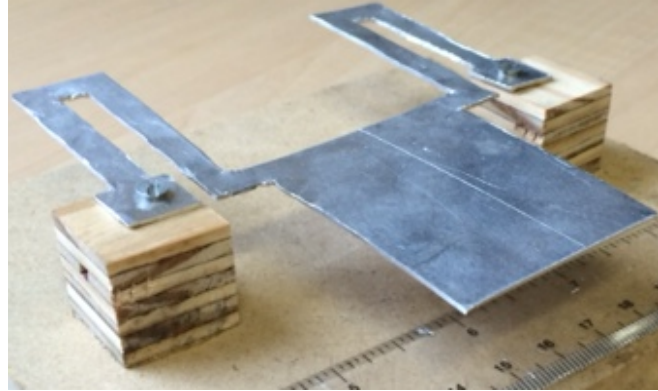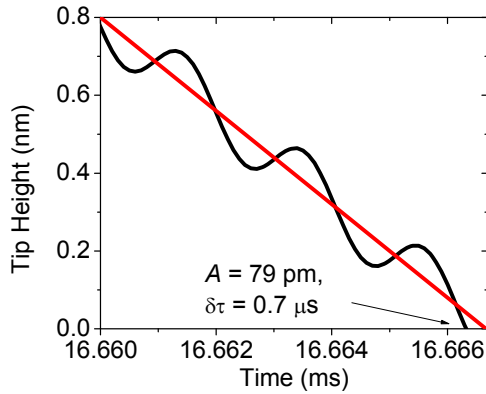

Fig. 6. (left) Tip height ramp vs time with superimposed vibrational noise at the natural frequency. (right) Scale aluminum model.

5. RESPONSIVITY

We follow the approach of [5]. The negative electrostatic pressure responsible for lifting the cantilever is proportional to the square of the electric field at the cantilever surface, and electric field should be proportional to the applied bias voltage V_B. According to [3], the electrostatic lifting force F_{ES} is inversely proportional to cantilever height z, and we find that FES can be approximated by the function

$$F_{ES} = (0.02 \text{ nN μm/V}^2) \; V_B^2/z \qquad . \tag{3}$$

Equating the elastic force $F_E = Kz$ to the electrostatic force F_{ES} gives the cantilever height as a function of applied voltage, according to

$$z = (0.0054 \text{ μm/V}) \; V_B \qquad . \tag{4}$$

The calculation of the thermal bimorph effect is the same as in [5], except that the considered device is smaller, with a total length including bimorph arms and paddle of 36 μm. Thus, including the bimorph effect, we find for a temperature change ΔT of the cantilever due to IR heating that

$$z = (0.0054 \text{ μm/V}) \; V_B - (0.017 \text{ μm/K}) \; \Delta T \qquad . \tag{5}$$

We find that an applied voltage $V_B = 400$ V is necessary to raise the cantilever to its horizontal position z = 2 μm. This is about 10x larger than the value at which dielectric breakdown is observed to occur. If we ignore this unpleasant detail, an applied bias saw tooth

$$
\begin{aligned}
V_B(t) &= 400 \text{ V } (1 - 60/\text{s } t) \qquad \text{for} \qquad t = 0 - 1/60 \text{ sec} \\
&= 0 \qquad\qquad\qquad\qquad\qquad\qquad t = 1/60 \text{ sec} - 1/30 \text{ sec}
\end{aligned}
\tag{6}
$$

cycles the cantilever over its full range of motion with a 50 % duty cycle at frame rate $FR = 30$ Hz. We then find that the time τ required for the cantilever to return to null position from its maximum height is

$$\tau = (1 - (0.0085/\text{K}) \; \Delta T)/(60/\text{s}) \qquad , \tag{7}$$

and the change in time of contact $\Delta\tau$ due to IR heating is then

$$\Delta\tau = 1.4 \times 10^{-4} \, \Delta T \qquad . \qquad . \qquad (8)$$

For the 0.3 ng oxide cantilever, we estimate a heat capacity C of 1.25×10^{-10} J/K using the Dulong-Petit value of 25 J/mol-K for specific heat. Then the adiabatic temperature change per unit absorbed power is

$$\Delta T_{ad}/\Delta P = 1/(C\,FR) = 2.6 \times 10^{8} \text{ K/W}. \qquad (9)$$

Allowing heat flow to the substrate through the bimorph and isolation arms, with total path length $L = 36$ µm, and thermal conductance $G = g\,t\,w\,/\,L$, where $g = 1$ W/m-K for the thermal conductivity, gives an equilibrium temperature rise for unit absorbed power under steady state illumination of

$$\Delta T_{eq}\,/\,\Delta P = 1/G = 2.2 \times 10^{7} \text{ K/W}. \qquad (10)$$

From Eqs. (8-10), we find responsivity R to be

$$R_{ad} = 37000 \text{ sec/W}, \qquad \text{and}$$
$$R_{eq} = 3100 \text{ sec/W}. \qquad (11)$$

6. NOISE EQUIVALENT POWER and NOISE EQUIVALENT TEMPERTURE DIFFERENCE

Noise equivalent power (NEP) is $N/(R\,f^{1/2})$, where N is the noise amplitude, R is the responsivity, and f is the bandwidth. We take $N = 660$ ns and $f = 20$ MHz. The latter will be justified below. Then

$$NEP_{ad} = 4.0 \times 10^{-15} \text{ W/rootHz}$$
$$NEP_{eq} = 4.8 \times 10^{-14} \text{ W/rootHz}. \qquad (12)$$

To estimate NETD, we integrate the derivative with respect to temperature of the Planck function from 8 to 12 microns wavelength, assuming typical collection optics and an $(18\ \mu m)^2$ absorbing area to find dP/dT_{scene} of 0.143 nW/K. Then from Eq. (11), we find that a 20 MHz bandwidth is required to resolve a 100 mK temperature difference in the scene for the worst case responsivity. From NETD = NEP $* f^{1/2}\,/\,(dP/dT_{scene})$ we find

$$NETD_{ad} = 0.13 \text{ K} \qquad \text{and}$$
$$NETD_{eq} = 1.5 \text{ K}. \qquad (13)$$

7. CONFIRMATION OF SPRING CONSTANT

The estimate of thermomechanical noise presented here depends on accurate estimation of the cantilever spring constant. The value we used was based on an FEM calculation, and there is reason to check this against results from analytic calculations and experiment. For a force concentrated at one end of a beam, the spring constant K has the value $(Ewt^3)/(4L^3)$, where w is the width, t the thickness of the arms, E Young's modulus, and L the length of the arms. We ignore the elbow and isolation arms, since experiment with models and FEM calculations show that most of the deformation occurs in the bimorph arms that attach to the absorber plate. The width w is taken to be the combined width of both bimorph arms together, or $w = 4$ µm, their thickness $t = 0.4$ µm, and $L = 18$ µm. Young's modulus for oxide is E = 70 GPa, which is nearly identical to the value for gold, which forms a thin layer on the oxide, so that we ignore this layer. Thus, we find that K = 0.79 N/m. This is 14% larger than the value 0.68 N/m found from the FEM calculation that considered the full structure and uniformly distributed force over the rigid paddle.

To further test the calculations, we fabricated a model that was intended to be dynamically similar to the MEMS device. In other words, the model should have the same spring constant as the actual device. To achieve this, the relative dimensions of the model are very different, i.e. it is not a scale model. An aluminum strip $E = 73$ GPa was fabricated with $L = 485$ mm, $w = 5$ mm, and $t = 1$ mm. The calculated spring constant of this strip is 0.76 N/m, which we consider

"close enough" to the 0.79 N/m value calculated by the same formula for the device. Tip displacement was measured as a function of applied force (using weights), and the spring constant was found to be 0.49 N/m. In other words, the textbook formula overestimated the actual spring constant by 35%. The FEM value exceeds the experimental value by 28%.

Several other simple thin aluminum rods with rectangular cross sections were measured and calculated. Measured spring constants were smaller than analytically calculated values by from zero to 26%. Measured values were smaller than FEM values by 45% for mesh dimensions that were half the smallest rod dimension. For larger meshes, FEM values were even larger, giving the sense that for sufficiently small mesh, the FEM values would converge to the experimental values.

Another mechanical test was done using an aluminum 2500x scale model of the device, pictured in Fig. 6 (right). The deformation when force was applied to the paddle qualitatively confirms the behavior determined by the FEM calculation (Fig. 5), i.e. that the elbows go up when the paddle goes down. The spring constant obtained was 1023 N/m. This result was compared to that from FEM and analytical calculations for the model. The FEM spring constant obtained was 1196 N/m. Again, the calculated value exceeded the experimental value, this time by 14%. The analytical calculation gave 1867 N/m, which exceeds the experimental value by 45%.

The conclusion from these comparisons between mechanical models and calculations is that FEM values tend to somewhat overestimate the actual spring constants, but they are at least the right order of magnitude. This is important, because we essentially have only the FEM value for the actual MEMS device, the simple rod model for analytic calculations being obviously a crude calculation. Thus, our obtained values of NEP and NETD are lower bounds, and actual IR detector performance is likely to be somewhat worse than estimated here.

8. SUMMARY

This paper analyzed thermomechanical noise for a novel IR detector based on null switching in a MEMS cantilever device. Because of the unusual method of operation, by which absorbed IR is transduced to a measurement of a time, high electronic bandwidth is required to achieve high sensitivity to small temperature differences in the scene. Thus, thermal vibrations at the natural frequency are important. The timing uncertainty, and hence noise, is primarily determined by the noise amplitude. NETD is found to lie between 1.5 and 0.13 K for ~20 μm pitch.

ACKNOWLEDGMENTS

REFERENCES

[1] Edwards, O., "Radiant energy imager using null switching", US patent 7977635 B2 (2011).
[2] Rezadad, I., Boroumand, J., Smith, E. M., Peale, R. E., "MEMS cantilever with electrostatically-controlled tip contact", in revision, Appl. Phys. Lett. (2014).
[3] Rezadad, I., Boroumand, J., Smith, E. M., Alhasan, A., Peale, R. E., "Vertical electrostatic force in MEMS cantilever IR sensor," Proc. SPIE 9070 (2014).
[4] Alhasan, A., [Comparison Of Casimir, Elastic, Electrostatic Forces For A Micro-Cantilever], Masters Thesis, UCF, Orlando, (2014).
[5] Smith, E., Boroumand, J., Rezadad, I., Figueiredo, P., Nath, J., Panjwani, D., Peale, R. E., Edwards, O., "MEMS clocking-cantilever thermal detector," Proc. SPIE 8704 - 100 (2013).
[6] Boroumand Azad, J., Rezadad, I., Nath, J., Smith, E. and Peale, R. E., "Release of MEMS devices with hard-baked polyimide sacrificial layer", Proc. SPIE 8682, 868226 (2013).
[7] Riley F. W. [Mechanics of Materials], John Wiley &Sons, New York, p. 679 (1999).
[8] Heer, C.V. [Statistical Mechanics, Kinetic Theory, and Stochastic Processes], Academic Press, Inc., New York, 413-431 (1972).

[9] Dereniak, E.L. and Boreman, G.D., [Infrared Detectors and Systems], John Wiley and Sons, New York, 177-183 (1996).